ISSN- 2394-5125 VOL 5, ISSUE 07, 2018

AC/AC Modular Multilevel Converter Using HF Transformer Based on PSO Optimized PI Control Strategy

[1]*Dr. K.Suneeta Professor, kintalisuneeta@gmail.com*
[2]*Mr. V.Saidulu Assistant Professor, pecsaidulu.eee@gmail.com*
[3]*Mr. B.Raju Assistant Professor , banothu.raju12@gmail.com*
Department-EEE
Nagole Univerisity Engineering and Technology Hyderabad

Abstract: The main aim of this project is AC/AC Modular multilevel converter using high-frequency (HF) transformer based on Particle Swarm Optimization (PSO) based PI control strategy. The proposed converter has more advantages of modular design, high power density, no circulation current, good output voltage waveform quality. This converter has broad application prospects in the fields of high-voltage and high-power wind power generation, fractional frequency power transmission (FFTS) and power electronic transformer. The proposed converter topology can connect two three-phase AC systems with different frequencies and amplitudes directly. By introducing HF transformer, the direct series connection of input and output modules can be realized simultaneously, and the expensive industrial frequency transformer with large volume and weight can be removed. In order to achieve HF electrical isolation, the HF inversion of the output pulse is carried out at the inverter side to realize the HF output of the fundamental wave. After passing the HF transformer, the pulse is restored to the low-frequency output wave by the cycloconverter. The modulation scheme, PSO based PI control strategy and typical parameter design are developed. Furthermore, the feasibility of the proposed converter is verified by simulation results.

Keywords: Modular Multilevel Converter (MMC), Particle Swarm Optimization (PSO), High Frequency (HF) transformer

I.INTRODUCTION

Reduced access to fossil fuels heightens the urgency of switching power plants to renewable energy sources. Wind power has emerged as a feasible option in recent years due to its minimal environmental effect. Although offshore wind power is vital to helping the world meet its renewable energy target [1], research on the most efficient means of incorporating it into the grid is just getting started. Discovering a converter has been the driving force for all of our other efforts. The output voltages from wind turbines are becoming too high for a two- or three-stage converter to handle effectively. Since the turn of the century, modular multilevel converters (MMCs) have been extensively employed to develop new types of converters [2]. MMC originally appeared in HVDC (high-voltage direct-current) networks [3]. The extensive use of voltage source converter architecture is a result of its many benefits, which include its modular design, simplicity of scaling, high output voltage waveform quality, and exceptional power characteristics. The majority of recent MMC literature is structured around subjects like fundamental circuit architecture and parameter design, mathematical model construction and analysis, modulation technique, control strategy, computer simulation technology, experiment design, and industrial device implementation. The requirement to eliminate DC fault components and the cost of establishing an offshore converter station prevent HVDC from being widely used in MMCs [8]. To connect offshore wind power networks, the fractional frequency transmission system (FFTS [9, 10], also known as low frequency alternating current (LFAC) [11] transmission system) is proposed as a revolutionary method. In [12], we assess the current state of LFAC studies and offer several transmission components designs for an upcoming offshore LFAC project. LFAC is required to connect offshore wind farms to the electrical grid, as mentioned in [11]. The offshore converter facility would have otherwise been required to convert the low-frequency electrical energy being. Following this innovation, offshore wind power projects are now more dependable and less expensive to launch. The University of Colorado's R.W. Erickson and O.A. al Naseem developed a modular multilevel matrix converter in 2001 [13] that can transition between numerous matrix levels. (M3C). The modular, multi-level

ISSN- 2394-5125 VOL 5, ISSUE 07, 2018

architecture that has been the distinguishing feature of M3C is being further developed in addition to the high voltage and high capacity of its predecessor, MMC. The tight coupling between currents of various frequencies makes this a difficult topic to study. Normal power transmission is interrupted if the M3C connection breaks down at either end. For the M3C mathematical model, a control method was developed using an arm-power analysis. The described double-zero transformation. It is difficult to change the DC voltage in this way in real time. We present a successful dq coordinate-based decoupling control approach in [16]. Lennart Babushka and Axel Martens suggested a ground-breaking hexagonal modular multilevel converter (Hexverter) for high-voltage and high-power applications in 2011 [17], [18]. The number of branches needed to connect two three-phase AC systems with different frequencies and amplitudes is reduced from the twelve required by MMC and M3C to just six, resulting in smaller equipment and lower manufacturing costs. According to [19], each Hexverter branch's current flow is controlled by a coupling inductor. After demonstrating how state-space equations can be used to regulate the amount of energy released by a branch, these equations are modified for general application. Hexverter can only have one internal circulation channel due to its design [20, 21]. This indicates that under typical operating conditions, the system must adhere to rigorous reactive power constraints. The same number of modules are used in the Y-MMC AC/AC modular multilevel converter system as in the Hexverter, but there is no circulating current channel, resulting in a cheaper overall system cost. The nonlinear interconnection and damping assignment passivity-based control (IDA-PBC) method has been used to study two control systems, the Y-MMC. Numerous studies have focused on the optimization of controller parameters, the elimination of interference, and the elimination of unknowns in controller design, using techniques such fuzzy neural networks (FNN) [25], disturbance observation, and sliding mode These AC-to-AC converters are all united by this lack of isolation. To create electrical isolation between the IF and FF circuits, large IF transformers are needed. The IF transformer has a number of drawbacks, such as its high price, sizable bulk, relatively high loss, saturation, and sizable initial inrush current [28, 29]. If the IF transformer has a high impedance when working with nonlinear loads, the voltage drops and the voltage harmonic components may be increased. High-power, high-voltage AC/AC converters are widely used in asynchronous networking, offshore wind power, long-distance fractional frequency power transmission, subsea petroleum gas exploration, and the construction of a subsea power transmission and distribution system. High-power AC/AC converters are used in a wide range of industries to power motor drive devices, crush ore, roll out metal, and carry out a variety of other operations. These industries include rail transportation, mining, smelting, and shipbuilding. Based on these findings, we suggest the HFT-MMC, a novel type of AC/AC converter. This converter creates a single product that combines the MMC and HFT's exceptional features.

II. EXISTING SYSTEM

In Fig.1 we can see the HFT-MMC operating with a PI-based PWM controller. Because the bulky and expensive IF transformer is unnecessary, the IF and FF modules can be directly connected in series when an HF transformer is used. The IF and FF sides, on the other hand, are more likely to have harmonics.

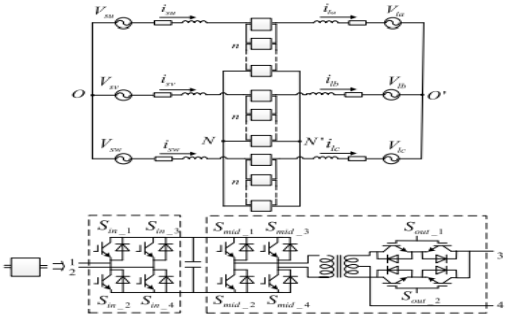

Fig 1 Circuit diagram of the HFT-MMC

III. PROPOSED SYSTEM

This research proposes a high-throughput multi-mode converter (HFT-MMC), as seen in Fig.2. A high power density, no circulating current, and a nearly perfect voltage waveform at the output are just a few of its many benefits. An HF transformer may be used to link the IF and FF modules in series, eliminating the need for a bulky, costly, and cumbersome IF transformer. In comparison to

ISSN- 2394-5125 VOL 5, ISSUE 07, 2018

conventional high-power AC/AC converters, the proposed design uses less parts, such as fewer branches, a lower overall IGBT capacity, and fewer capacitors. Each end of the planned HFT-MMC will house a single three-phase AC system with higher frequency and amplitude than the other. The letters U, V, and W stand for the endpoints of the IF and FF systems, whereas the letters asfs and fl denote the corresponding frequency ranges. Consequently, we may suppose that the IF side's three-phase voltages and currents are Vsu, Vsv, Vsw and isu, isv, isw, while the FF side's are Vla, Vlb, Vlc and ila, ilb, ilc, with neutral points O and O 0 on both sides. Phases u and an of the IF system are joined at the first fork in HFT-MMC, Phases v and b at the second fork, and Phases w and c at the third fork. Given that there are n distinct sub-modules, it may be split into four sections, one for each of the four potential forks. The H-bridge on the left, with its four switches, is the rectifier; the H-bridge in the center, with its two switches, is the inverter; and the H-bridge on the right, with its four switches, is the cycloconverter. The cycloconverter uses two anti-series IGBTs to build each bidirectional switch. The inverter and cycloconverter are linked via a high frequency (HF) transformer. A rectifier and an inverter work together to transform DC into AC in the standard AC/AC converter (DC to AC). The cycloconverter is operating in zero-voltage switching (ZVS) mode, which causes the secondary voltage of the HF transformer to remain at zero when the IGBT is turned on (see Part C of II for specific description). Since transformers are not counted when determining the number of energy conversion links in a power electronic converter, HFT-MMC may be thought of as a two-stage energy converter composed just of a rectifier and an inverter. By varying the number of connections, the recommended converter can switch between DC/DC, AC/DC, and DC/AC. The inverter bridge, the HF transformer, and the cycloconverter may be utilized as a DC power electronic transformer for DC/DC power transformation with HF electrical isolation if the rectifier bridge at the head end is omitted. Given its DC.

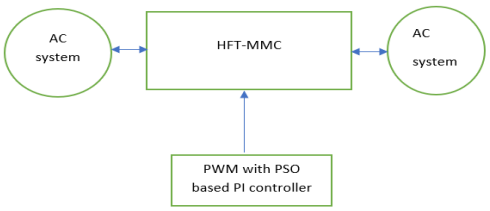

Fig. 2 Proposed block diagram of the HFT-MMC

MODULATION STRUCTURE

We employ some good old' fashioned carrier phase-shifted pulse width modulation at the rectifier end (CPS-PWM). Comparing a triangle carrier wave with a sinusoidal modulation signal that has the same frequency and amplitude but has been rotated at a specific angle is the first stage in the process. Figs. 3 and 4 display the circuitry for producing the trigger signal as well as the logic of the rectifier's IGBTs. The trigger signals for Sins 2 and 4 are produced using mirror images of Sins 1 and 3.

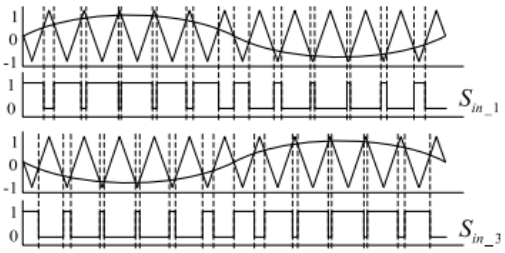

.

Fig.3 CPS-PWM signal generation

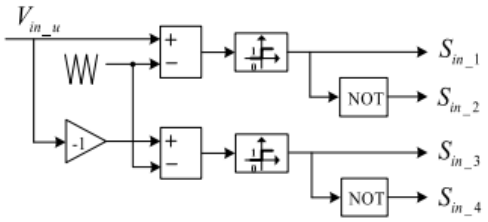

Fig.4 Rectifier trigger signal generation

The inverter circuit incorporates a selection link to produce trigger signals based on the constant power source pulse width modulation. Since the trigger signal for generations 1 and 3 is a rectangular pulse, we will use the triangular carrier wave used by Smid 1 as an illustration. If the synchronous

ISSN- 2394-5125 VOL 5, ISSUE 07, 2018

signal is 1, then G1 should be used as the trigger for Smid 1, and if it is G3, then G3 should be used. In order to activate Smid 3, G3 could be turned on only when the synchronous signal is 1, and off otherwise. It's common knowledge that CPS-PWM can switch between four distinct modes. When combined with G1, G3, and synchronous signals, our proposed pulse-width-modulation (PWM) of the inverter generates four distinct switching modes. This allows for higher frequency modulation of the inverter's output voltage and faster switching of the IGBTs. Inductors-Gate-Bridge-Transistors (IGBTs) and their associated logic and design are depicted in Figures 4 and 5 for your perusal. Table 1 displays all switch positions for the module.

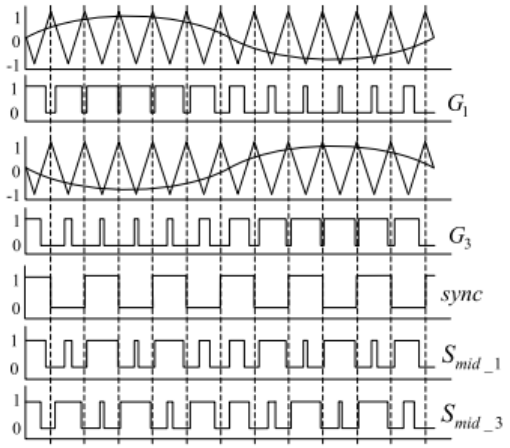

Fig.5 HF flip trigger signal generation

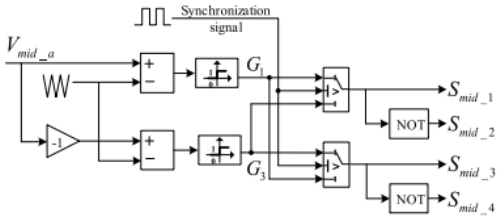

Fig.6 Inverter trigger signal generation

Two reverse-series IGBTs that are activated by the same signal make up each of the two bidirectional switches in the cycloconverter, which has two of them. The two bidirectional switches are activated by opposing pulses. As an illustration, the top bidirectional switch is "on" and the output voltage is the same as the input voltage when the trigger pulse is at its maximum level. When the trigger pulse is at a low level, the switch becomes unidirectionally off and the output voltage is positive in relation to the input voltage. The input HF voltage of the cycloconverter may be recovered through modulation. IGBTs in the cycloconverter may switch when the input voltage is zero (ZVS) for pulse restoration operation if the inverter and cycloconverter use the same synchronous square wave signal.

Table-1 Switching states of the inverter

Signals	Switching States							
G_1	1	1	0	0	1	1	0	0
G_2	1	0	0	1	1	0	0	1
Sync	0	0	0	0	1	1	1	1
S_1	1	0	0	1	1	1	0	0
S_2	0	1	1	0	0	0	1	1
S_3	1	1	0	0	1	0	0	1
S_4	0	0	1	1	0	1	1	0
V	0	-	0	+	0	+	0	-

IV. CONTROL STRATAGY

Control system for inner loop

To achieve our goals, we use a feedforward dq decoupling-based control technique. You can learn more about the history of the inner loop controller we're using now by reading here,

$$V_{sd\_fs} = V_{sd} - Ri_{sd} - L\frac{di_{sd}}{dt} + \omega_s Li_{sq} = V_{sd} + \omega_s Li_{sq} - K_P(i_{sd\_ref} - i_{sd}) - K_I \times \int (i_{sd\_ref} - i_{sd})dt \quad (1)$$

$$V_{sq\_fs} = V_{sq} - Ri_{sq} - L\frac{di_{sq}}{dt} - \omega_s Li_{sd} = V_{sq} - \omega_s Li_{sd} - K_P(i_{sq\_ref} - i_{sq}) - K_I \times \int (i_{sq\_ref} - i_{sq})dt \quad (2)$$

$$V_{ld\_fl} = V_{ld} + Ri_{ld} + L\frac{di_{ld}}{dt} - \omega_l Li_{lq} = V_{ld} - \omega_l Li_{lq} + K_P(i_{ld\_ref} - i_{ld}) + K_I \times \int (i_{ld\_ref} - i_{ld})dt \quad (3)$$

$$V_{lq\_fl} = V_{lq} + Ri_{lq} + L\frac{di_{lq}}{dt} + \omega_l Li_{ld} = V_{lq} + \omega_l Li_{ld} + K_P(i_{lq\_ref} - i_{lq}) + K_I \times \int (i_{lq\_ref} - i_{lq})dt \quad (4)$$

ISSN- 2394-5125 VOL 5, ISSUE 07, 2018

Control system for outer loop

When the HFT-MMC converter is connected to the grid, conventional methods of controlling power and voltage may be used to complete the external loop and regulate output voltage and current. As a result, either constant DC voltage control or constant AC voltage control may be employed in the IF side system, and either may be utilized in the FF side system. Since the method's comprehensive derivation can be found in other studies, we will not go into depth about it here despite its widespread application. When the converter's control mode is set to constant V/F islanding, the output voltage source frequency may be changed from 0 to 50 Hz.

Balance control system for inner-arm

As the parameter values and switching periods of the modules in a branch are not similar, the modules will experience varied charging and discharging conditions from the branch current, resulting to an imbalance in the capacitance voltage across the branch. Capacitance voltage in the branch may be equalized using a modulation wave correction-based voltage equalization management approach, provided the branch's external voltage characteristics remain stable.

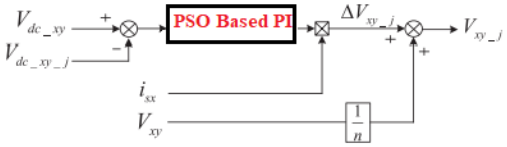

Fig.7 Balancing control system for inner-arm

Figure 4 is a control block diagram showing how an inner-arm balancing method is used to achieve rectifier side symmetry in this study. Current flowing through the branch is denoted by Isx, average DC voltage in arm xy as Vdc xy, module j's capacitance voltage as Vdc xy j, module voltage after adjustment as 1Vxy j, and branch voltage as Vxy. You can get the adjusted voltage's exact value if you, it is

$$V_{xy\_j} = \frac{V_{xy}}{n} + \Delta V_{xy\_j} = \frac{V_{xy}}{n} + K_p(V_{dc\_xy} - V_{dc\_xy\_j})i_{sx} \quad (5)$$

The voltage of the module capacitance increases when a positive correction is used to make up for a module with below-average DC voltage because the correction voltage is in phase with the branch current, which pumps energy into the capacitor. When the DC voltage is higher than average, a negative adjustment shortens the charging time, which causes the capacitor to discharge and causes the capacitance voltage of the module to decrease accordingly. Indicated in is the full branch voltage distribution (6). It is clear that none of the branches' output features were impacted by the adjustment.

$$\begin{aligned} V_{xy} + \sum_{j}^{n} \Delta V_{xy\_j} &= V_{xy} + \sum_{j}^{n} K_p(V_{dc\_xy} - V_{dc\_xy\_j})i_{sx} \\ &= V_{xy} + nK_p i_{sx}(V_{dc\_xy} - \frac{1}{n}\sum_{i}^{n} V_{dc\_xy\_j}) \\ &= V_{xy} \end{aligned} \quad (6)$$

The modulation and control strategy stated above may be used to construct the control system depicted in Fig. 4.8. An ABC/dq transformation is done to the dq components of the voltages and currents measured on the IF and FF sides in order to simplify operations. In response to the current directives from the voltage/power control, the control blocks' inner loop current control produces the modulation signals. The final modulation signals may be synthesized from a variety of frequency components once the modulation signals in the ABC frame have been revealed by the dq/ABC transformation.

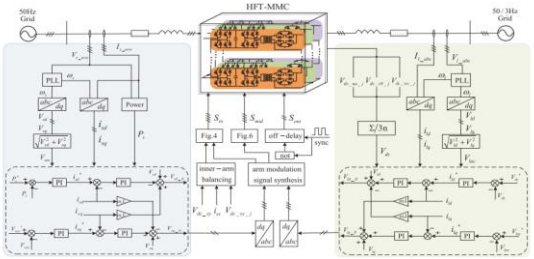

Fig.8 HFT-MMC Control system

V. PSO

Particle swarm optimization (PSO) is inspired by studies of animal social behavior. Birds in the air and schools of fish in the water are two examples. PSO might use the experience gathered to choose

ISSN- 2394-5125 VOL 5, ISSUE 07, 2018

the best course of action. Each possible solution in PSO's search space is represented by a "bird." The term "particle" describes its little size and solitary nature. Movement of particles is determined by their velocities, and their fitness (and hence their health) is maximized using a fitness function. The issue is resolved when particles swiftly follow the best particles through the trouble spot. To find the best solution, particle swarm optimization (PSO) starts with a large population of random particles (solutions) and iteratively tweaks the parameters that govern the next generation. At each cycle, the state of the particles is changed by taking the mean of the two "best" values. Research so far suggests that choice 1 is the best course of action. (Your physical activity is also recorded.) This portable is often referred to as a "Pbest." The particle swarm optimizer, like the heuristic optimizer, retains score by tallying up the best particle performances. The highest possible grade is Gbest, and it really is the best.

To provide just one example, the i.th particle in a d-dimensional space may be represented by the equation x i=. (x i1,x i2,.....x I d). Here, the most likely previous position of the ith particle is recorded and shown as

$$P_{best_i} = (P_{best_{i1}}, P_{best_{i2}}, \dots \dots P_{best_{id}}) \quad (7)$$

gbest is an index that is used to find the best particle in a set. An expression for v i= describes the velocity of particle I. (v I 1, v I 2, v I 3, etc.) Applying the particles' current velocities to the distance from Pbest-id yields their new velocities and locations. for gbest-id.

$$v_{i,m}^{(t+1)} = wv_{i,m}^{(t)} + c_1 rand()(P_{best_{i,m}} - x_{i,m}^{(t)}) + c_2 rand()(g_{best_m} - x_{i,m}^{(t)}) \quad (8)$$

$$x_{i,m}^{(t+1)} = x_{i,m}^{(t)} + v_{i,m}^{(t+1)} \quad (9)$$

$i = 1,2, \dots \dots \dots \dots n;$

$m = 1,2, \dots \dots \dots \dots d;$

Where:

n - Number of particles in the group,

d - Dimension,

t - Pointer of iterations (generations),

$v_{i,m}^{(t)}$ -Velocity of particle i at iteration t ,

w - Inertia weight factor,

c_1 , c_2- Acceleration constant,

rand ( ) - Random number between 0 and 1,

$v_{i,d}^{(t)}$- Current position of particle i at iterations,

P_{best_i}- Best previous position of the i.th particle,

g_{best} - Best particle among all the particles in the Population.

The evolution of PSO algorithms is seen across time in Figure 3. The first step in PSO is to create seed populations. Humans are made up of a collection of codes called chromosomes. The "fitness function" or performance index of a population also offers this sort of evaluation. When one takes care of their health in this way, not only does their health improve, but so does their quality of life. At some point after determining the fitness value and the generation number, the evolution process is stopped (Maximum iteration number reached?). Find out the particle- and population-level Pbest and gbest values. Particle data such as speed, position, best g and p values, and optimal start and end points are all adjusted.

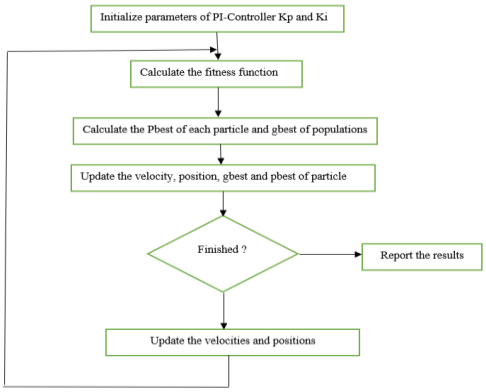

Fig.9 PSO algorithm

VI. SIMULATION RESULTS

ISSN- 2394-5125 VOL 5, ISSUE 07, 2018

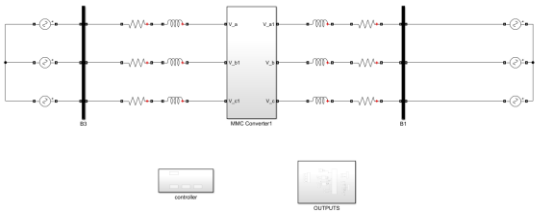

Fig.10 MATLAB/SIMULINK circuit diagram of the system

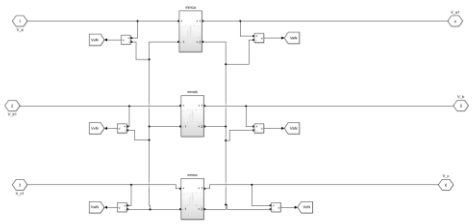

Fig.11 Subsystem of MMC

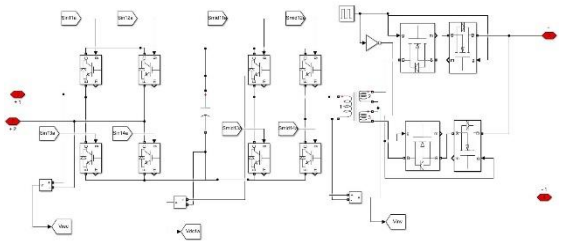

Fig.12 Subsystem module of MMC

A) EXISTING RESULTS

A. STEADY STATE SIMULATION OF HFT-MMC

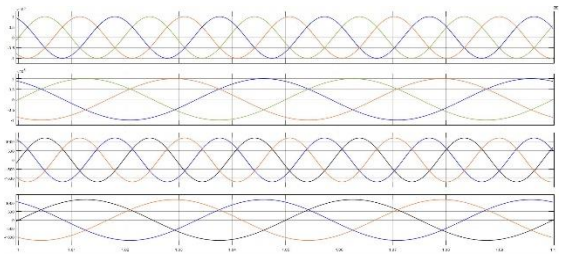

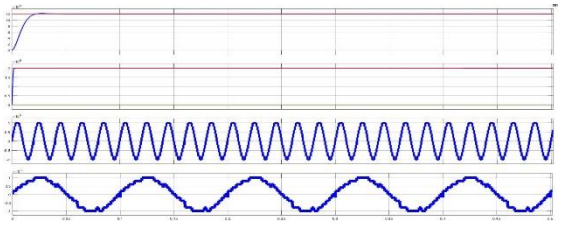

FIGURE.13 Steady-state simulation results of HFT-MMC's external characteristics. (a) Three-phase voltages of IF side and FF side [V]. (b) Three-phase currents of IF side and FF side [A]. (c) Average equivalent DC voltage [V]. (d) The active and reactive power transferred between both ends [W, Var]. (e) Branch voltages of IF side and FF side [V].

Fig.14 THD% voltage at industrial frequency (IF) side is 3.83%

Fig.15 THD% current at industrial frequency (IF) side is 5.73%

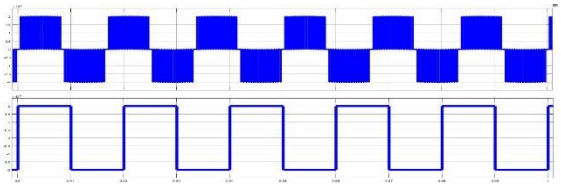

FIGURE 16 Frequency conversion of voltages from rectifier to cyclo-converter (a) Rectifier input

ISSN- 2394-5125 VOL 5, ISSUE 07, 2018

line voltage [V]. (b) Inverter output line voltage [V].

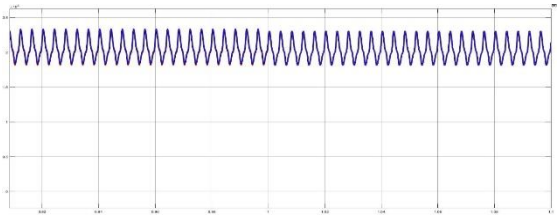

FIGURE.17 DC voltages of 6 sub-modules in branch ua [V].

B. DYNAMIC PERFORMANCE OF HFT-MMC

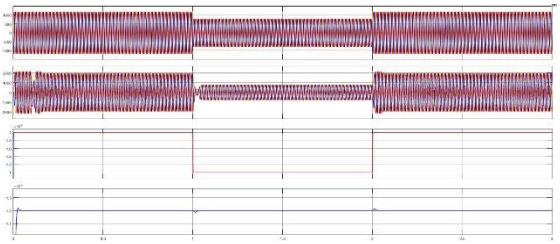

FIGURE.18 Dynamic Performance of HFT-MMC. (a) Three-phase currents of IF side and FF side [A]. (b) DC-link voltage [V]. (c) The input active power and reactive power of converter from IF system [W, Var].

C. THREE PHASE SYMMETRICAL GRID FAULT OF IF SYSTEM

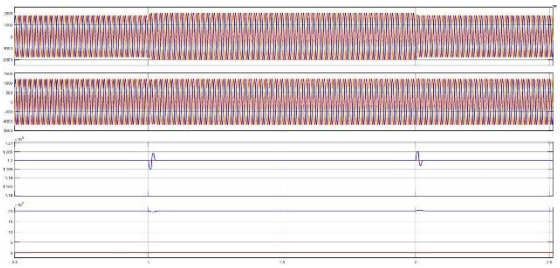

FIGURE.19 Symmetrical grid fault simulation results of HFT-MMC. (a) Three-phase current of IF side and FF side [A]. (b) Average value of equivalent DC voltage [V]. (c) The input active power and reactive power of converter from IF system [W, Var].

D. ASYMMETRICAL GRID FAULT OF IF SYSTEM

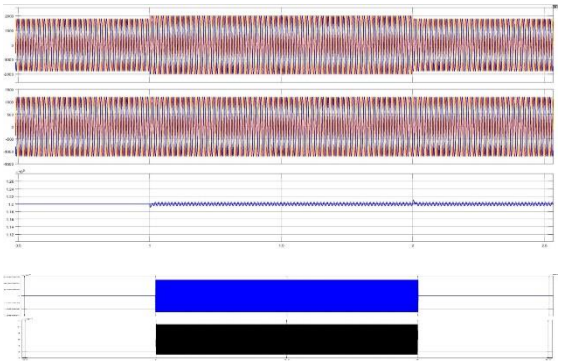

FIGURE .20 Asymmetrical fault simulation results of HFT-MMC. (a) Three-phase currents of IF side and FF side [A]. (b) Average value of equivalent DC voltage [V]. (c) The input active power and reactive power of converter from IF system [W, Var].

B) EXTENSION RESULTS

A. STEADY STATE SIMULATION OF HFT-MMC

We offer static simulations of HFT-MMC in Fig.21 to highlight its outwardly obvious properties. Voltages for the IF and FF phases in three phases are shown in Fig.21 (a). The IF and FF three-phase currents are shown in Figure.21 (b). each side maintains appropriate power quality, and the three-phase symmetry is maintained. The DC voltage may be quickly and easily stabilized to be very close to the target value, as shown in Fig.21 (c). A voltage ripple of less than 2% indicates that the capacitance value was properly adjusted to guarantee the steady functioning of the system. Using a 200 MW active power and a 0 MVar reactive power (operating at unity power factor), Fig.21 depicts the constant flow of active and reactive power between the terminals (d). Consistently excellent performance is shown in steady state, with power variations of less than 0.5 MW and 1% amplitude. The single-phase branch voltages on the IF and FF sides of the distribution transformer are shown in Fig.21 (e). Figures 22 and 23 depict the THD% of voltage and current on the IF side of industry.

ISSN- 2394-5125 VOL 5, ISSUE 07, 2018

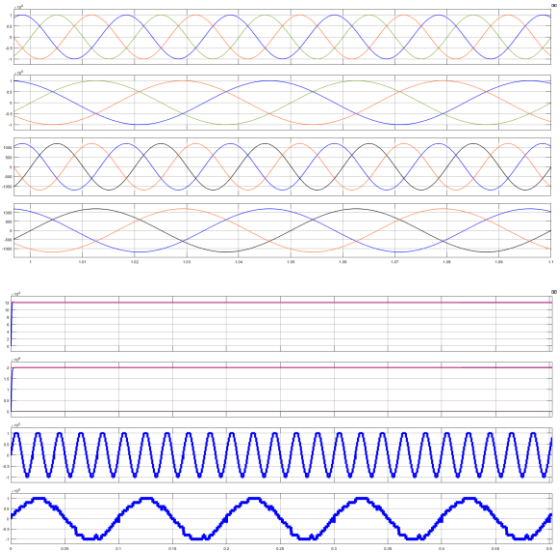

FIGURE.21 Steady-state simulation results of HFT-MMC's external characteristics. (a) Three-phase voltages of IF side and FF side [V]. (b) Three-phase currents of IF side and FF side [A]. (c) Average equivalent DC voltage [V]. (d) The active and reactive power transferred between both ends [W, Var]. (e) Branch voltages of IF side and FF side [V].

Fig.22 THD% voltage at industrial frequency (IF) IF side is 0.41%

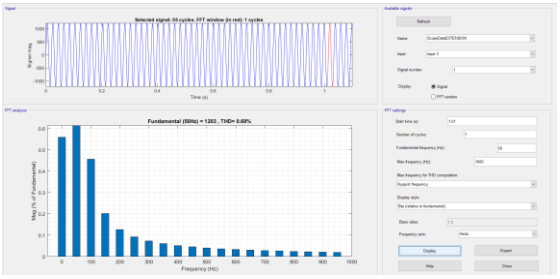

Fig.23 THD% current at industrial frequency (IF) side is 0.69%

B. DYNAMIC PERFORMANCE OF HFT-MMC

Due to the likelihood that the load and power supply connected to the system would fluctuate during regular operation, changing the power passing through the converter, a dynamic performance assessment of the proposed system is also required. We initially lower the active power reference from 200 to 100 MW at t = 1 s and then boost it from 100 to 200 MW at t = 2 s to evaluate the performance of HFT-reactive MMC. Fig.24 displays an illustration of the performance of the HFT-dynamic MMC, which was made feasible by the parties' almost immediate replies.

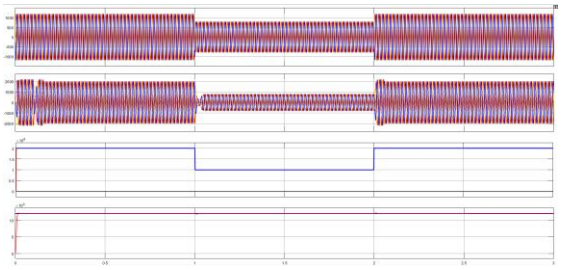

FIGURE.24 Dynamic Performance of HFT-MMC. (a) Three-phase currents of IF side and FF side [A]. (b) DC-link voltage [V]. (c) The input active power and reactive power of converter from IF system [W, Var].

C. THREE PHASE SYMMETRICAL GRID FAULT OF IF SYSTEM

The IF and FF currents are shown in Fig 25. (a). As soon as the fault is repaired, the IF fault current rapidly decreases to normal levels. Problems on the IF side have negligible effects on the FF side in terms of current and voltage amplitude. Very little shift in average DC voltage or transmission power was observed during the fault (Fig.25 (b) and.25(c)). This research shows that the suggested preventative measure works. The results of a fault simulation from phase a to the ground are shown in Fig 25. At t = 1 s, the IF side voltage indicating phase u drops to 0.6 p.u., but by t = 2 s, it has recovered to 1.0 p.u. For what it's worth, I haven't seen any changes in the way regulations are being enforced.

ISSN- 2394-5125 VOL 5, ISSUE 07, 2018

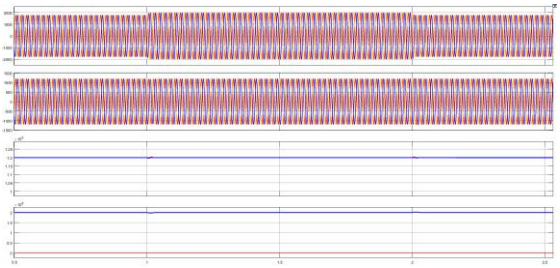

FIGURE.25 Symmetrical grid fault simulation results of HFT-MMC. (a) Three-phase current of IF side and FF side [A]. (b) Average value of equivalent DC voltage [V]. (c) The input active power and reactive power of converter from IF system [W, Var].

D. ASYMMETRICAL GRID FAULT OF IF SYSTEM

For a graphic illustration of the IF and FF currents, see Fig.26 (a)When a defect arises, the IF side current's three-phase symmetry is momentarily broken, but it is soon restored once the issue has been fixed. On the FF side, the three-phase currents are very imbalanced. The average DC voltage varies by less than 1%, but is still very steady, as seen in Fig.26 (b). Power fluctuations from the IF system are present at the converter's input during the fault, as depicted in Fig. 26(c), but these power fluctuations disappear once the fault has been fixed.

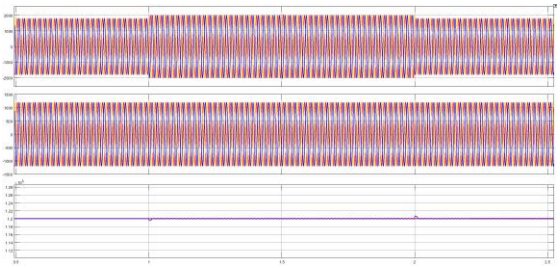

FIGURE.26 Asymmetrical fault simulation results of HFT-MMC.

COMPARISION TABLE

	Existing system (With PI controller)	Extension system (With PSO optimized PI controller)
Voltage THD% at IF side	3.83%	0.41%
Current THD at IF side	5.73%	0.69%

CONCLUSION

This paper proposes a new AC/AC converter using MMC and HF transformer based on PSO optimized. It has the following characteristics: 1) The converter realizes galvanic isolation by utilizing HF transformers. 2) On the basis of CPS-PWM, an improved PWM modulation method is used to generate the modulation signals at the inverter side, which realizes the HF control of the inverter output voltages, after passing the HF transformer, the cycloconverter restore the pulses to the low-frequency output voltage. 3) By adding the common conduction time between two groups of IGBTs of the cycloconverter, the freewheeling of the HF link can be solved preliminarily. 4) The dq decoupling control strategy is adopted to realize the stable control of the proposed converter. The simulation results revealed the effectiveness of the proposed PSO based PI control topology. As observed the simulation results the proposed system gives less THD% compared to existing system.

REFERENCES

[1] Assessing the EU 2030 Climate and Energy Targets, ECOFYS, Utrecht, The Netherlands, 2014.

[2] A. Lesnicar and R. Marquardt, ‘‘An innovative modular multilevel converter topology suitable for a wide power range,’’ in Proc. IEEE Bologna Power Tech Conf., Bologna, Italy, vol. 3, Jun. 2003, p. 6.

[3] Z. Li, P. Wang, H. Zhu, Z. Chu, and Y. Li, ‘‘An improved pulse width modulation method for chopper-cell-based modular multilevel converters,’’ IEEE Trans. Power Electron., vol. 27, no. 8, pp. 3472–3481, Aug. 2012.

[4] M. A. Perez, S. Bernet, J. Rodriguez, S. Kouro, and R. Lizana, ‘‘Circuit topologies, modeling, control schemes, and applications of modular

ISSN- 2394-5125 VOL 5, ISSUE 07, 2018

multilevel converters,'' IEEE Trans. Power Electron., vol. 30, no. 1, pp. 4–17, Jan. 2015.

[5] J. Bocker, B. Freudenberg, A. The, and S. Dieckerhoff, ''Experimental comparison of model predictive control and cascaded control of the modular multilevel converter,'' IEEE Trans. Power Electron., vol. 30, no. 1, pp. 422–430, Jan. 2015.

[6] M. Saeedifard and R. Iravani, ''Dynamic performance of a modular multilevel back-to-back HVDC system,'' IEEE Trans. Power Del., vol. 25, no. 4, pp. 2903–2912, Oct. 2010.

[7] Q. Song, W. Liu, X. Li, H. Rao, S. Xu, and L. Li, ''A steady-state analysis method for a modular multilevel converter,'' IEEE Trans. Power Electron., vol. 28, no. 8, pp. 3702–3713, Aug. 2013.

[8] P. Bresesti, W. L. Kling, R. L. Hendriks, and R. Vailati, ''HVDC connection of offshore wind farms to the transmission system,'' IEEE Trans. Energy Convers., vol. 22, no. 1, pp. 37–43, Mar. 2007.

[9] X. Wang and X. Wang, ''Feasibility study of fractional frequency transmission system,'' IEEE Trans. Power Syst., vol. 11, no. 2, pp. 962–967, May 1996.

[10] W. Xifan, C. Chengjun, and Z. Zhichao, ''Experiment on fractional frequency transmission system,'' IEEE Trans. Power Syst., vol. 21, no. 1, pp. 372–377, Feb. 2006.

[11] W. Fischer, R. Braun, and I. Erlich, ''Low frequency high voltage offshore grid for transmission of renewable power,'' in Proc. 3rd IEEE PES Innov. Smart Grid Technol. Eur. (ISGT Europe), Oct. 2012, vol. 1, no. 6, pp. 14–17.

[12] J. Ruddy, R. Meere, and T. O'Donnell, ''Low frequency AC transmission for offshore wind power: A review,'' Renew. Sustain. Energy Rev., vol. 56, pp. 75–86, Apr. 2016.

[13] R. W. Erickson and O. A. Al-Naseem, ''A new family of matrix converters,'' in Proc. 27th Annu. Conf. IEEE Ind. Electron. Soc. (IECON), vol. 2, Nov./Dec. 2001, pp. 1515–1520.

[14] W. Kawamura, M. Hagiwara, and H. Akagi, ''A broad range of frequency control for the modular multilevel cascade converter based on triple-star bridge-cells (MMCC-TSBC),'' in Proc. IEEE Energy Convers. Congr. Expo., Denver, CO, USA, Sep. 2013, pp. 4014–4021.

[15] W. Kawamura, M. Hagiwara, and H. Akagi, ''Control and experiment of a modular multilevel cascade converter based on triple-star bridge cells,'' IEEE Trans. Ind. Appl., vol. 50, no. 5, pp. 3536–3548, Sep./Oct. 2014.

[16] S. Liu, X. Wang, Y. Meng, P. Sun, H. Luo, and B. Wang, ''A decoupled control strategy of modular multilevel matrix converter for fractional frequency transmission system,'' IEEE Trans. Power Del., vol. 32, no. 4, pp. 2111–2121, Aug. 2017.

[17] L. Baruschka and A. Mertens, ''A new 3-phase AC/AC modular multilevel converter with six branches in hexagonal configuration,'' in Proc. IEEE Energy Convers. Congr. Expo., Phoenix, AZ, USA, Sep. 2011, pp. 4005–4012.